frontiers in Chemistry

ORIGINAL RESEARCH
published: 17 December 2020
doi: 10.3389/fchem.2020.616468

Different Benzendicarboxylate-Directed Structural Variations and Properties of Four New Porous Cd(II)-Pyridyl-Triazole Coordination Polymers

Ying Zhao[1†], *Jin Jing*[2†], *Ning Yan*[2], *Min-Le Han*[1], *Guo-Ping Yang*[2*] *and Lu-Fang Ma*[1*]

[1] College of Chemistry and Chemical Engineering, Luoyang Normal University, Luoyang, China, [2] Key Laboratory of Synthetic and Natural Functional Molecule of Ministry of Education, Shaanxi Key Laboratory of Physico-Inorganic Chemistry, College of Chemistry & Materials Science, Northwest University, Xi'an, China

OPEN ACCESS

Edited by:
Feng Luo,
East China University of Technology, China

Reviewed by:
Dongsheng Li,
China Three Gorges University, China
Zhao Junwei,
Henan University, China

***Correspondence:**
Lu-Fang Ma
mazhuxp@126.com
Guo-Ping Yang
ygp@nwu.edu.cn

[†] These authors have contributed equally to this work

Specialty section:
This article was submitted to Inorganic Chemistry, a section of the journal Frontiers in Chemistry

Received: 12 October 2020
Accepted: 16 November 2020
Published: 17 December 2020

Citation:
Zhao Y, Jing J, Yan N, Han M-L, Yang G-P and Ma L-F (2020) Different Benzendicarboxylate-Directed Structural Variations and Properties of Four New Porous Cd(II)-Pyridyl-Triazole Coordination Polymers. Front. Chem. 8:616468. doi: 10.3389/fchem.2020.616468

Four new different porous crystalline Cd(II)-based coordination polymers (CPs), i. e., $[Cd(mdpt)_2]\cdot 2H_2O$ (**1**), $[Cd_2(mdpt)_2(m\text{-bdc})(H_2O)_2]$ (**2**), $[Cd(Hmdpt)(p\text{-bdc})]\cdot 2H_2O$ (**3**), and $[Cd_3(mdpt)_2(bpdc)_2]\cdot 2.5NMP$ (**4**), were obtained successfully by the assembly of Cd(II) ions and bitopic 3-(3-methyl-2-pyridyl)-5-(4-pyridyl)-1,2,4-triazole (Hmdpt) in the presence of various benzendicarboxylate ligands, i.e., 1,3/1,4-benzenedicarboxylic acid (m-H_2bdc, p-H_2bdc) and biphenyl-4,4′-bicarboxylate (H_2bpdc). Herein, complex **1** is a porous 2-fold interpenetrated four-connected 3D ***NbO*** topological framework based on the $mdpt^-$ ligand; **2** reveals a two-dimensional (2D) ***hcb*** network. Interestingly, **3** presents a three-dimensional (3D) rare interpenetrated double-insertion supramolecular net *via* 2D ···ABAB··· layers and can be viewed as an ***fsh*** topological net, while complex **4** displays a 3D ***sqc117*** framework. Then, the different gas sorption performances were carried out carefully for complexes **1** and **4**, the results of which showed **4** has preferable sorption than that of **1** and can be the potential CO_2 storage and separation material. Furthermore, the stability and luminescence of four complexes were performed carefully in the solid state.

Keywords: coordination polymers, structural variations, topologies, gas adsorption, luminescent properties

INTRODUCTION

The coordination polymers (CPs) have gained considerable research interest by the self-assembly of various organic linkers (including different functional groups) with metal ions/clusters due to their special topological nets and broad applications (Wang et al., 2014, 2015; Smith et al., 2015; Wang and Wang, 2015; Dey et al., 2017; Hong et al., 2017; Islamoglu et al., 2017; Kariem et al., 2017; Lin et al., 2017; Li et al., 2018; Xing and Janiak, 2020; Zhang et al., 2020). Generally, the coordination preference of the nature of ligands and geometries of ions are the primary considerations in the preparation process of CPs. However, other factors, such as the choice of auxiliary ligands, pH,

template effect, as well as reaction temperature, etc., are considered to be the great roles in the fabrications of the desired structures (Chen et al., 2015; Song et al., 2015; Waller et al., 2015; Blandez et al., 2016; Lannoeye et al., 2016; Manna et al., 2016; Rosa et al., 2016; Lu et al., 2017). Besides, the typical non-covalent supramolecular interlocks, including H-bonding, $\pi\cdots\pi$ stacking, etc., may also help to fine-tune the structural assemblies (Wheeler, 2013; Yadav and Gorbitz, 2013; Bhattacharya et al., 2014, 2016; DeFuria et al., 2016; Ju et al., 2016; Li et al., 2016, 2017; Song et al., 2016; Yao et al., 2016; Park et al., 2017). Thus, it is essential to explore these factors to further help study the relationship of structures and properties.

The current research findings have presented that N-containing heterocyclic ligands possess excellent binding abilities with different center metal ions to construct various CPs. Further, most of them may be acted as the neutral building units and also as the anionic units by releasing the acidic N-H groups of the ligands, showing more versatile coordination fashions (Lin et al., 2010, 2011; Chen et al., 2013; Li et al., 2019). Recently, there are some studies mainly focused on the N-heterocycles and their derivatives with five-membered rings (including the imidazole, triazole, or tetrazole groups, etc.) and multicarboxylate as mixed ligands to build different porous CPs (Pachfule and Banerjee, 2011; Chen et al., 2013; Liu et al., 2014; Qin et al., 2014; Wang et al., 2014; Du et al., 2015; Li et al., 2016, 2017; Yan et al., 2017), which often show exceptional gas sorption and luminescent performances. Similarly, the phenlycarboxylate tectons have also been proven to be the great candidates to yield functional CPs because of their abundant coordination modes with ions (Chen et al., 2013; Li et al., 2015; Jin et al., 2016; Wu et al., 2017).

As a combination of the above stated facts and our previous works, a rigid N-heterocyclic 3-(3-methyl-2-pyridyl)-5-(4-pyridyl)-1,2,4-triazole (Hmdpt) ligand was deliberately chosen with three kinds of phenyldicarboxylate linkers, i.e., 1,3/1,4-benzenedicarboxylate (*m*-H_2bdc, *p*-H_2bdc) and biphenyl-4,4′-dicarboxylate (H_2bpdc) to prepare porous CPs in this study. The Hmdpt tecton has lots of coordination sites and also can be the excellent hydrogen bonding donor/acceptor in the assembly of new CPs. Herein, four new Cd(II)-CPs, $[Cd(mdpt)_2]\cdot 2H_2O$ (**1**), $[Cd_2(mdpt)_2(m\text{-}bdc)(H_2O)_2]$ (**2**), $[Cd(Hmdpt)(p\text{-}bdc)]\cdot 2H_2O$ (**3**), as well as $[Cd_3(mdpt)_2(bpdc)_2]\cdot 2.5NMP$ (**4**), were synthesized successfully. Complex **1** displays a 2-fold interlocked four-connected ***NbO*** framework; **2** reveals a two-dimensional (2D) ***hcb*** network. More interestingly, complex **3** presents a three-dimensional (3D) rare interlocked double-insertion ***fsh*** supramolecular net *via* 2D ···ABAB··· layers, while **4** is a 3D ***sqc117*** network. Their structural diversity indicates that the different secondary benzendicarboxylate linkers have great influence on the assembly process of new CPs. The stability and luminescence were investigated carefully for four complexes in the solid state. Especially, the different gas sorption performances have been carried out for **1** and **4** in detail, indicating **4** has preferable adsorption than that of **1** and can be the potential CO_2 capture/separation material.

EXPERIMENTAL SECTION

Materials and General Methods

All the reagents/solvents were brought to use in the experiments with no further purification. The characterization methods of the four complexes are given in section Materials and General Methods. Because the synthesis processes of four CPs are very similar, thus the synthesis of CP **1** is only presented herein briefly, and others can be found in the supporting information.

Synthesis of $[Cd(mdpt)_2]\cdot 2H_2O$ (**1**). A mixture of $3CdSO_4\cdot 8H_2O$ (0.05 mmol, 38.5 mg), Hmdpt (0.05 mmol, 11.8 mg), DMA (4 ml), and H_2O (6 ml) was mixed in a 25-ml Teflon-lined stainless steel vessel, which was heated at 120°C for 72 h and then cooled to room temperature at the rate of 10°C/h to form colorless block crystals. Yield is 63% (based on Hmdpt). Elemental analysis of **1**, calculated (%): C 51.75, N 23.22, H 3.98; found: C 51.68, N 23.38, H 3.73. Fourier Transform Infrared spectra (FT-IR) (cm^{-1}): 3,525 (m), 3,436 (m), 3,244 (m), 1,612 (m), 1,424 (m), 1,110 (s), 839 (w), 716 (w), 608 (s).

X-Ray Crystal Structure Determinations

The instruments used for X-ray crystallographic measurements and the refinement methods and details by SHELXL-97 (Sheldrick, 1997) are displayed in section X-Ray Crystal Structure Determinations. The crystallographic data of four CPs are listed in **Table 1**. The Cambridge Crystallographic Data Centre (CCDC) numbers of the four CPs are 1543594–1543597, respectively.

RESULTS AND DISCUSSION

Structure Description of $[Cd(mdpt)_2]\cdot 2H_2O$ (1)

Based on the X-ray single-crystal diffraction of complex **1**, it crystallizes in the *R*-3 trigonal system. Each Cd(II) ion is coordinated octahedrally with 2-pyridyl/triazolate N atoms from two $mdpt^-$ linkers as the *trans* fashion as well as 4-pyridyl N atoms from the adjacent units (**Figure 1A**), and the similar complex of which has been reported before (Lin et al., 2010). The Cd–N lengths are the 2.215–2.408 Å, and the angles *via* Cd(II) center are 71.27° (8)—180.0°.

The $mdpt^-$ linker holds two coordination fashions, i.e., bridged/chelated bidentate fashions ($\eta^1\mu_1\chi^1$ and $\eta^2\mu_1\chi^2$) in **1**, to coordinate with Cd(II) ions (**Figure 1B** and **Supplementary Figure 4**) to form a porous 3D framework (**Figure 1C**), and the void volume ratio of which is about 23.2% after exclusion of the guest water molecules by the calculation of PLATON program. Topologically, each ligand links two Cd(II) centers and each Cd(II) center joins four different bridged linkers, respectively. Thus, complex **1** displays a 2-fold four-connected interpenetrating ***NbO*** topological type with the $(6^4.8^2)$ point symbol (**Figure 1D**).

Structure Description of $[Cd_2(mdpt)_2(m\text{-}bdc)(H_2O)_2]$ (2)

When the different carboxylate ligands are introduced in the reaction systems, Cd(II) centers are more prone to coordinate

TABLE 1 | Crystal data and refinements of four complexes.

Complexes	1	2	3	4
Formula	$C_{26}H_{24}CdN_{10}O_2$	$C_{34}H_{28}Cd_2N_{10}O_6$	$C_{21}H_{19}CdN_5O_6$	$C_{66.5}H_{58.5}Cd_3N_{12.5}O_{10.5}$
Mass	602.93	897.48	549.81	1,537.66
Crystal system	Trigonal	Monoclinic	Monoclinic	Monoclinic
Space group	*R*-3	$P2_1/c$	$P2_1/n$	*C2/c*
a [Å]	27.122 (4)	21.920 (2)	9.9364 (12)	30.332 (4)
b [Å]	27.122 (4)	7.1964 (8)	14.6653 (18)	11.0553 (13)
c [Å]	10.7626 (17)	30.860 (2)	15.4981 (19)	21.499 (3)
α [°]	90	90	90	90
β [°]	90	134.521(4)	103.739 (2)	114.604 (2)
γ[°]	120	90	90	90
V [Å^3]	6856 (3)	3470.9 (5)	2193.8 (5)	6554.7 (14)
Z	9	1	4	4
$D_{calcd.}$[g·cm^{-3}]	1.275	1.710	1.665	1.307
μ [mm^{-1}]	0.747	1.286	1.044	1.015
F [000]	2646	1768	1104	2552
GOOF	1.069	1.182	1.014	1.019
$R_1{}^a$ [I>2σ(I)]	0.0292	0.0418	0.0235	0.0488
$wR_2{}^b$ (all data)	0.0699	0.1603	0.0840	0.1661

$^aR_1 = \sum||F_o|-|F_c||/\sum|F_o|$, $^bwR_2 = [\sum w(F_o^2 - F_c^2)^2/\sum w(F_o^2)^2]^{1/2}$.

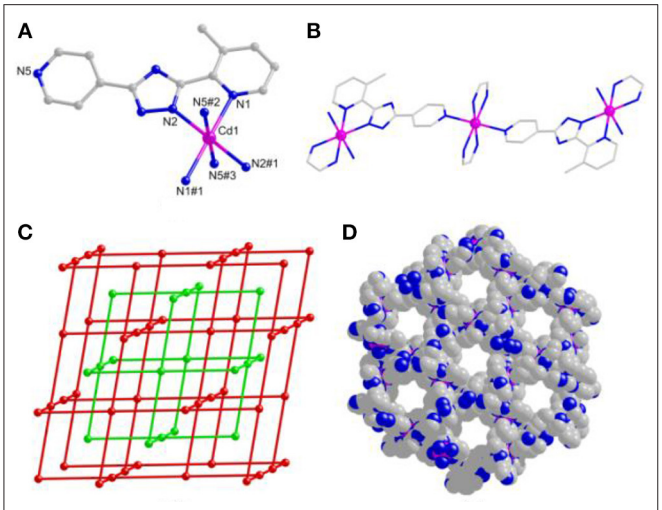

FIGURE 1 | (A) The Cd(II) coordination geometry of **1**. **(B)** One-dimensional (1D) chain-like motif of **1**. **(C)** Three-dimensional (3D) space-filling view of **1**. **(D)** Topological representation of **1**.

with O atoms than N atoms *via* the soft–hard acid–base (SHAB) principle, thus making various dimensionalities and structures of complexes (Zhang S. et al., 2013; Zhang X. et al., 2013). Herein, complex **2** has the $P2_1/c$ monoclinic system. The asymmetric unit holds two independent Cd(II) centers, two mdpt$^-$, one *m*-bdc^{2-} linker, as well as two coordinated waters. All the Cd(II) ions have the hexa-coordinated geometries and possess the similar modes to link different ligands. Each Cd(II) center makes coordination with two O atoms of one *m*-bdc^{2-}, one O atom of water molecule, and three N atoms of two different mdpt$^-$ tectons (**Figure 2A**). The Cd–O/Cd–N distances are 2.272–2.434/2.267–2.371 Å, respectively; and the angles *via* Cd(II) ion are 55.49°-175.63° (**Supplementary Table 1**).

In **2**, Cd(II) ions are connected through mdpt$^-$ ligand to give rise to a 1D wave-like motif (**Figure 2B**). These adjacent 1D chains are further extended by *m*-bdc^{2-} tectons to yield a waved 2D layered structure along the *a* axis (**Figure 2C**). Topologically, each mdpt$^-$ and *m*-bdc^{2-} linker two Cd(II) centers, which can be regarded as three-connected nodes, thus, the 2D structure can be viewed as a three-connected (6^3) ***hcb*** net (**Figure 2D**). In addition, there exist the different hydrogen H-bonding interlocks ($N_2\cdots O_5$, $N_7\cdots O_6$) in the adjacent parallel 2D networks, which help to combine these 2D motifs as a final 3D supramolecular structure (**Figure 3**).

Structure Description of [Cd(Hmdpt)(*p*-bdc)]·2H$_2$O (3)

Compared with the *m*-H_2bdc ligand, the distance of the carboxylate groups of *p*-H_2bdc is much farther to each other, which thus results in the various mode with Cd(II) centers and structure of **3**. Compound **3** has the $P2_1/n$ monoclinic system. The building block consists of a Cd(II) center, an Hmdpt, a *p*-bdc^{2-} tecton, and two guest waters. Each Cd(II) center adopts a seven-coordinated environment in which four O atoms are from the same *p*-bpc^{2-} and three N atoms are derived from two Hmdpt linkers (**Figure 4A**). The Cd–N/Cd–O lengths are 2.363∼2.374/2.329∼2.5175Å, and the angles *via* Cd(II) ion are 53.56–162.80° (**Supplementary Table 1**).

In **3**, the N atoms of Hmdpt ligand adopt 2-pyridyl and triazolate 1-nitrogens chelating and 4-pyridyl bridging modes

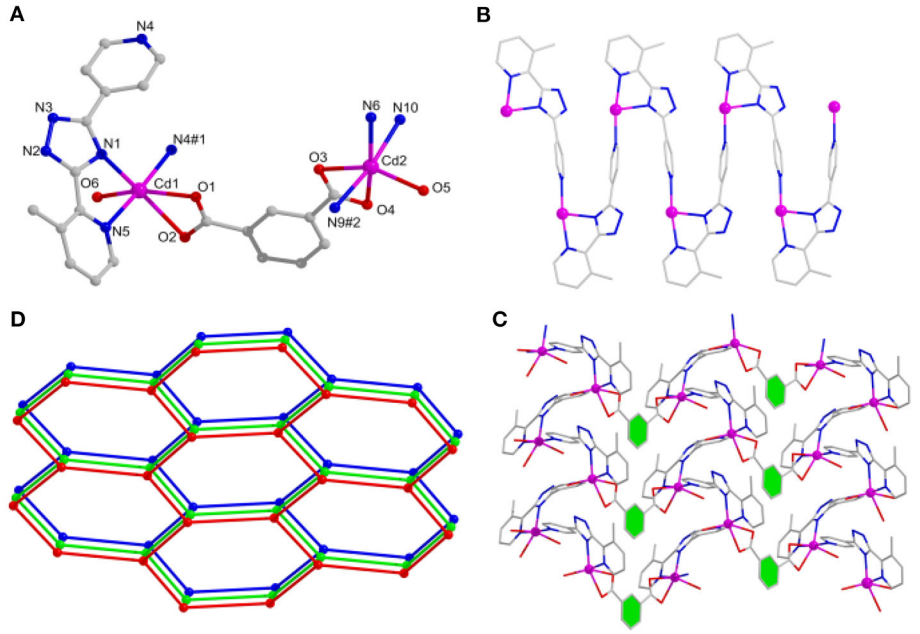

FIGURE 2 | (A) The Cd(II) coordination environments of **2**. **(B)** One-dimensional (1D) chain motif of **2** along *a* axis. **(C)** Two-dimensional (2D) layered structure of **2**. **(D)** Topological net of **2**.

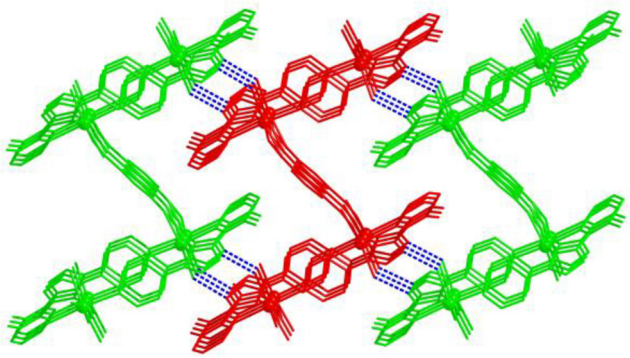

FIGURE 3 | The intermolecular H-bonding interlocks between the two-dimensional (2D) layers, yielding a three-dimensional (3D) supramolecular motif along *c* axis.

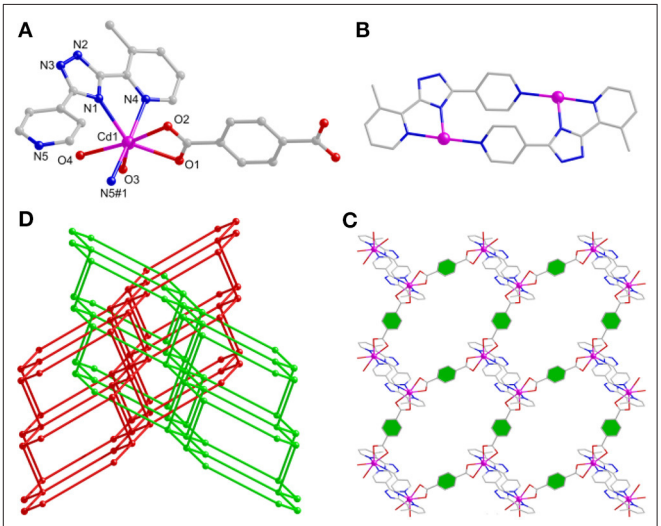

FIGURE 4 | (A) The Cd(II) coordination geometry of **3**. **(B)** The binuclear unit of **3**. **(C)** The two-dimensional (2D) layered motif of **3** *via* the *a* axis. **(D)** The 2-fold interlocked topology of **3**.

with two Cd(II) ions, forming a secondary building unit $[Cd_2(mdpt)_2]$ (**Figure 4B**), which produced an infinite 1D chain motif through *p*-bdc^{2-} ligand (**Supplementary Figure 1**). The neighboring 1D chains were successfully bridged by *p*-bdc^{2-} linkers to produce a new 2D layer via the *a* axis (**Figure 4C**). Like that of complex **2**, although **3** is also a 2D layered motif, however, the 2D layers are characterized by the accumulation of ···ABAB··· fashion. Further, the hydrogen bonds between the AA layers and water molecule O_6 form a 3D supramolecular network and then interpenetrate with the 3D net held by the BB layers (**Supplementary Figure 2**). When the topological method is employed for analyzing the structure, complex **3** can be simplified as (4,6)-connected ***fsh*** framework, and the point symbol of which is $(4^3.6^3)_2(4^6.6^6.8^3)$ (**Figure 4D**).

Structure Description of $[Cd_3(mdpt)_2(bpdc)_2]$·2.5NMP (4)

Due to the distance of two carboxylate groups of H_2bpdc longer than those of **3**, thereby, a 3D dense framework of **4** is

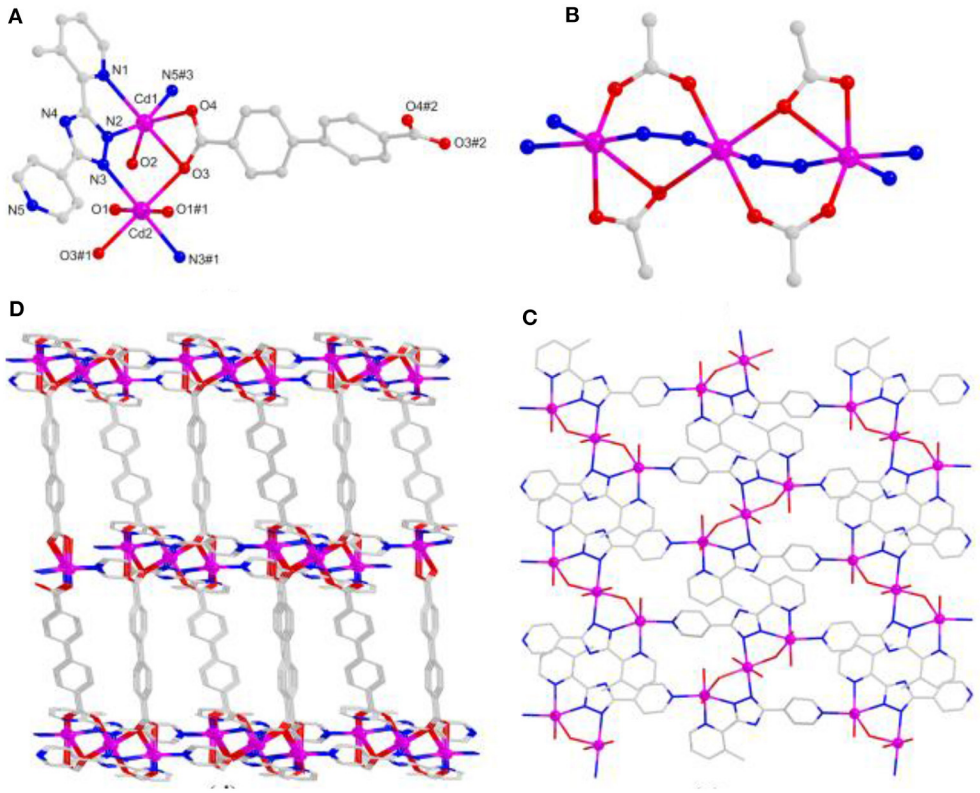

FIGURE 5 | (A) The Cd(II) coordination geometries of **4**. **(B)** The $[Cd_3(\mu_2\text{-}COO)_4N_4]$ SBU of **4**. **(C)** The two-dimensional (2D) layered motif based on $mdpt^-$ tectons of **4** via the *a* axis. **(D)** The three-dimensional (3D) porous structure of **4** via the *b* axis.

formed. Complex **4** crystallizes in the monoclinic *C*2/c crystal system. There contain three kinds of Cd(II) centers, two $mdpt^-$ tectons, as well as two $bpdc^{2-}$ linkers to form the asymmetric unit. The Cd–O/Cd–N distances are 2.185–2.613/2.229–2.395 Å, respectively.

Due to the twist of the two benzene rings, which makes the Cd1 and Cd2 centers adopt the same hexa-coordinated geometries but different coordination environments, where the Cd1 center takes coordination with three O atoms of bridging $bpdc^{2-}$ tectons and three N atoms of $mdpt^-$ linkers, the Cd2 center is bonded with four O atoms of bridging $bpdc^{2-}$ tectons as well as two N atoms of $mdpt^-$ linkers (**Figure 5A**). The deprotonated carboxylates exhibit $\eta^2\mu_2\chi^3$ and $\eta^2\mu_2\chi^2$ (**Supplementary Figure 5**) coordination modes and the N2, N3 of the $mdpt^-$ ligands are coordinated with three Cd(II) ions to result in a new $[Cd_3(\mu_2\text{-}COO)_4N_4]$ secondary building unit (SBU) (**Figure 5B**). Such SBUs are further bridged by $mdpt^-$ tectons to afford a 2D $[Cd_3(mdpt)_2]$ layered motif along the *a* axis (**Figure 5C**). Moreover, these 2D adjacent motifs are further supported by introducing the flexible $bpdc^{2-}$ linkers as the pillars to produce a 3D porous pillar-layered framework along the *b* axis (**Figure 5D**). As shown in **Supplementary Figure 4**, a pore space-filling structure is presented, and the void ratio is about 32.9% based on the PLATON program calculation. From a topological viewpoint, each Cd SBU may be simplified as the eight-connected nodes, and the overall net thus forms a $(3^6.4^{12}.5^8.6^2)$ ***sqc117*** net (**Figure 6**).

From the above structural features of four CPs, it can be found that the different auxiliary tectons may give rise to the new structural variations and then further help to fine-tune the properties of CPs. In the same reaction systems, the minor differences of the ligands will make great changes in the assembly processes of CPs, the benefit of which should be explored carefully to control the fabrications of new CPs with desired structures and performances.

Powder X-Ray Diffraction Measurement and Thermal Stabilities

The mass identities and phase purity of the four complexes were tested by comparisons of the experimental and the simulated powder X-ray diffraction (PXRD) patterns from the X-ray single-crystal data (**Supplementary Figure 6**), indicating the high-quality crystalline products.

The Thermogravimetric analysis (TGA) data were also tested carefully for studying the stability of the four complexes (**Supplementary Figure 7**). It is found that complex **1** firstly loses its guest waters in ∼30–113°C [observed (obsd.) ∼5.9%, calculated (calcd.) ∼4.7%] and then collapse the linkers gradually. For complex **2**, a plateau is observed from the beginning to 30°C and then a ∼3.3% loss in ∼30–201°C, which

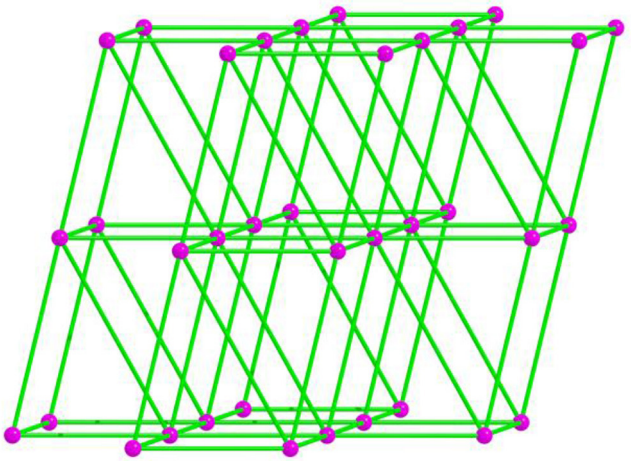

FIGURE 6 | The topological framework of **4**.

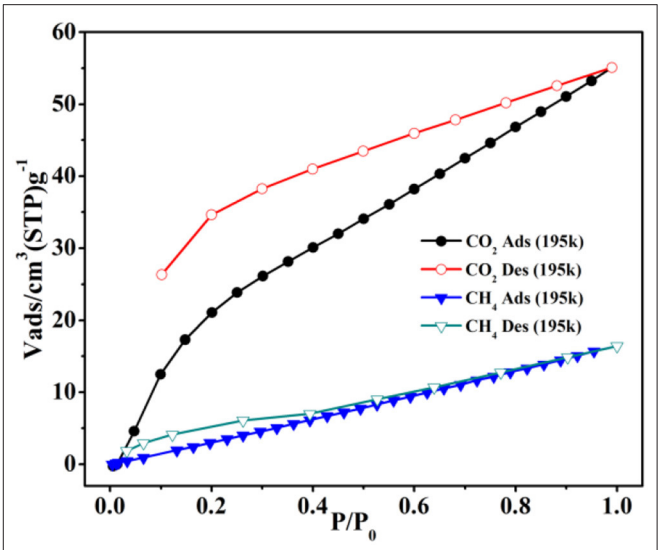

FIGURE 7 | The CO_2/CH_4 sorption isotherms of **1a** at 195K.

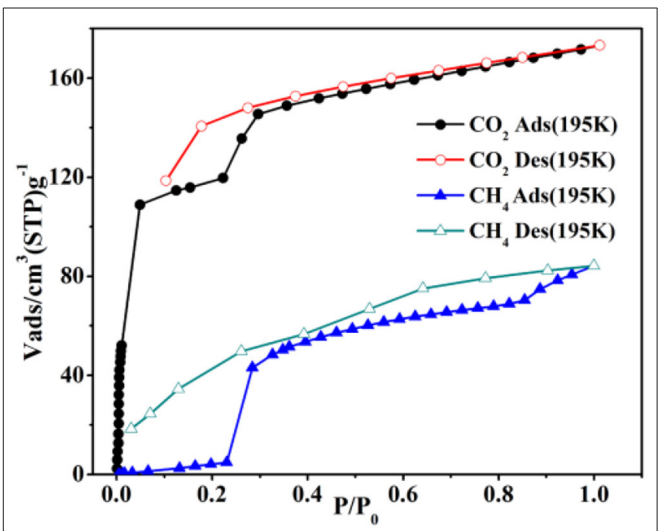

FIGURE 8 | The CO_2/CH_4 sorption isotherms of **4a** at 195K.

matches well with the removal of two coordinated waters (calcd. ∼4.0%); the second ∼22% loss appears in ∼315–366°C, which is attributed to a collapsed *m*-H_2bdc ligand, and then the rest of the ligand starts to decompose gradually. Complex **3** loses guest waters in ∼30–100°C (obsd. ∼6.3%, calcd. ∼6.6%), then follows a plateau of stability to ∼306°C, and then an abrupt 29% loss in ∼306–349°C, matching with the *p*-bdc loss (calcd. ∼30%). Complex **4** incurs a ∼15.4% loss in ∼30–267°C for reduction in all NMP molecules (calcd. ∼16.1%), then holds the stability to ∼357°C.

Gas Sorption of Complexes 1 and 4

The gas capture isotherms were tested carefully to prove the void properties of **1** for CO_2 and CH_4. The crystalline product of **1** was soaked in CH_2Cl_2 for 24 h and then dried under vacuum at 80°C to afford the desolvated **1a**. The gas captures of **1a** were performed carefully at 195 and 273K, respectively. At 1 atm, the uptake amount is 55.1 cm^3 g^{-1} (1.08 wt.%) for CO_2 (**Figure 7**), which is greatly higher than the CH_4 uptake (16.4 cm^3 g^{-1}, 0.12 wt.%) at 195K. The gas sorption of CO_2/CH_4 was also performed at 273K (**Supplementary Figure 9**), and the CO_2/CH_4 uptake is 29.6/11.0 cm^3 g^{-1} (0.58/0.08 wt.%) at 1 atm, respectively. Interestingly, the hysteresis effect is found for the CO_2 sorption of **1a**, the reason of which might be the interactions of framework with CO_2 to hinder the CO_2 from the host framework in the sorption/desorption procedure (Biswas et al., 2013; Boldog et al., 2013; Liang et al., 2013; Han et al., 2017). Further, the PXRD patterns still closely matched well with the stimulated patterns of **1** (**Supplementary Figure 6**), indicating that the sample after heating retained the intact host framework.

Compared with complex **1**, **4** has preferable adsorption property, which may arise from introducing auxiliary H_2bpdc ligand to give rise to more active sites and the flexibility of two benzene rings. Thus, the sorption isotherms were measured for $N_2/CO_2/CH_4$ to verify the porosity of **4**. Herein, **4** is soaked in CH_2Cl_2 for 24 h and dried at 150°C under vacuum to yield the desolvated crystalline product (**4a**) successfully, which is proved by the combination of the TGA and FT-IR tests (**Supplementary Figure 8**). At 77K and 1 atm, the N_2 uptake is 8.74 cm^3 g^{-1} and the capture isotherm has an obvious hysteresis in the sorption/desorption process (**Supplementary Figure 10**).

At 195K and 1 atm, the CO_2 sorption has a higher capture amount (34.04 wt.%, 173.28 cm^3 g^{-1}) to further prove the pore performances of **4a**. The Brunner-Emmet-Teller (BET) and Langmuir surface areas are 273.65/382.56 m^2 g^{-1}. Interestingly, the CO_2 sorption exhibits a double abrupt increase at 0.04, 0.22 atm as a significant hysteretic desorption curve (**Figure 8**). In the initial step, the CO_2 sorption amount is adsorbed as 109 cm^3 g^{-1} (21.41 wt.%) for **4a**, and then the isotherm has a sudden increase in the second step ($P/P_0 = 0.2$) and finally keeps the saturation.

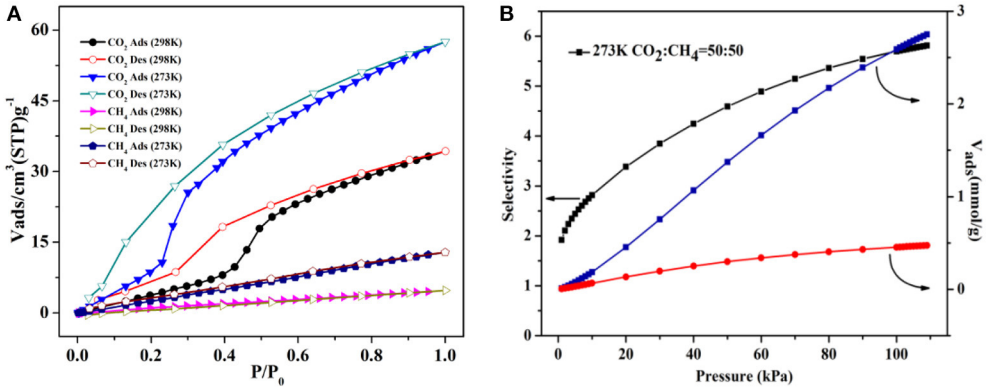

FIGURE 9 | (A) The CO_2/CH_4 isotherms of **4a** at 273/298K. **(B)** The ideal adsorbed solution theory (IAST) selectivity for equimolar CO_2/CH_4 mixture at 273K.

The desorption process does not retrace the capture process, which shows the different hysteresis, and the amount is 119 $cm^3\ g^{-1}$ ($P/P_0 = 0.1$) at the end of desorption. The incomplete desorption suggests there exist the interactions of CO_2 and pore surface. Generally, this phenomenon in rigid metal-organic framework (MOFs) may be ascribed to the sorbate/sorbent interlocks as the gases capture by surfaces of the structure, obtaining the various pores as it breathes (Bezuidenhout et al., 2015; Ichikawa et al., 2016; Esfandiari et al., 2017). When at relatively lower pressures, the two distorted benzene groups of $bpdc^{2-}$ ligand make the pore open, thus, leading to a rather large hysteresis.

The sorption isotherm of CH_4 shows a lower amount (6.02 wt.%, 84.19 $cm^3\ g^{-1}$) at 195K and 1 atm (**Figure 8**). However, it has a more obvious abrupt step with two sudden increases at 0.22/0.85 atm, which is similar to the CO_2 isotherm. The CO_2 is captured as 3.08 wt.% (43.23 $cm^3\ g^{-1}$) for **4a** in the initial step, and then the isotherm holds a sharp increase ($P/P_0 > 0.85$) and finally keeps the saturation. And the desorption process also displays the several steps at the corresponding points. As a result, the large hysteresis loops happen, leading that the CH_4 is packed in the structure at the lower pressures and not released right now on decreasing the external pressure (Liu et al., 2013; Handke et al., 2014; Ju et al., 2015; Hiraide et al., 2017; Sun et al., 2017).

The CO_2/CH_4 sorption properties of **4a** were also explored at 273/298K. The CO_2 uptake amounts are 57.53 $cm^3\ g^{-1}$ (11.3 wt.%) and 34.28 $cm^3\ g^{-1}$ (6.7 wt.%) at 273/298 K, 1 atm (**Figure 9A**), and the CH_4 amounts are 12.83 $cm^3\ g^{-1}$ (0.9 wt.%) and 4.75 $cm^3\ g^{-1}$ (0.3 wt.%) at 273/298K. These results indicate that **4a** has the selectivity for CO_2 molecules, which is more evident at the higher temperature. Thus, the CO_2/CH_4 selectivity of **4a** is calculated by ideal adsorbed solution theory (IAST) at 273K (Chen et al., 2015) (**Supplementary Figure 11**). Here, the CO_2/CH_4 molar fraction is set as 50/50 to simulate the content of biogas mixture (**Figure 9B**). The results present that CO_2 selectivity rapidly ascends with increasing load for both mixed contents over CH_4, and the selectivity CO_2/CH_4 is calculated as 5.7 from the equimolar gas phase mixture at 1 atm.

The capture enthalpy (Q_{st}) was estimated to explore the CO_2 affinity via the Virial equation of sorption isotherms at 273K (**Supplementary Figure 12**), revealing **4a** has a higher CO_2 affinity at high loading amount. The Q_{st} has a slow decrease by the CO_2 increasing capture; however, it is 23.2 kJ mol^{-1} at the final (**Figure 10**). This value is comparable to those of the hydrated HKUST-1, MAF-2, JUC-132, JLU-Liu, and NOTT-140 (30, 27, 30, 30, and 25 kJ/mol), but higher than those of most "benchmark CPs," such as CuBTTri, MOF-5, and UMCM-1 (21, 17, 12 kJ/mol) (Wang et al., 2015) Thereby, complex **4** may be explored as a great gas adsorbent in many fields.

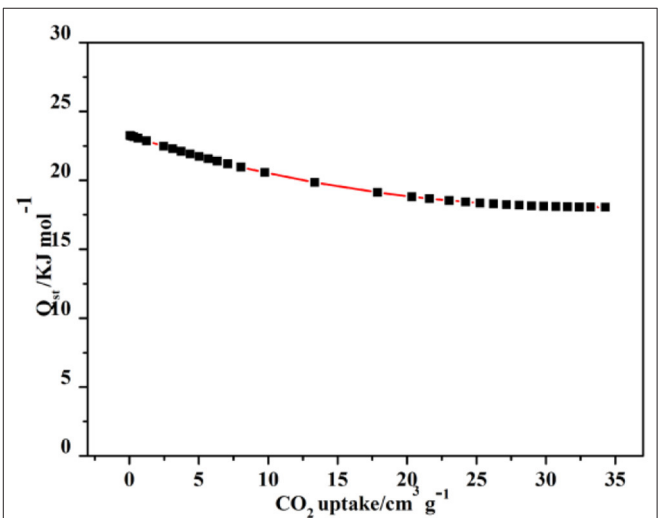

FIGURE 10 | The CO_2 Q_{st} of **4a** at 273K.

Luminescent Properties

Due to the great luminescent performances of the Hmdpt linker and d^{10} complexes (Chou et al., 2014; Kumar et al., 2014; Hu et al., 2015; Ye et al., 2015; Wang et al., 2016; Hong et al., 2017; Lim et al., 2017), the solid-state photoluminescence properties have been studied for the four complexes and Hmdpt as well as the various auxiliary benzendicarboxylates at room temperature (**Figure 11** and **Supplementary Figure 13**), the emissions of

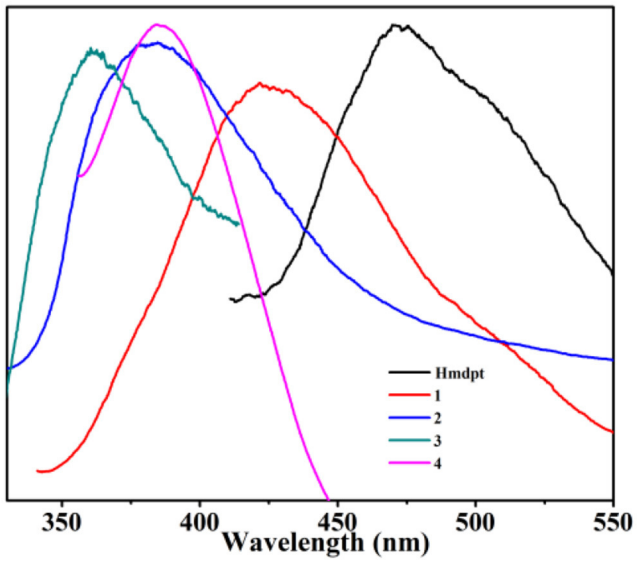

FIGURE 11 | The solid-state luminescent emission spectra of the four coordination polymers (CPs) and Hmdpt linker.

which are given in **Supplementary Table 2**. The free Hmdpt shows the band at 472 nm when excited at 307 nm, attributing to the $\pi^* \rightarrow \pi$ transition of the intra-ligand (Lin et al., 2017). The four complexes have their specific emissions, the bands of which were presented at 425 nm ($\lambda_{ex} = 321$ nm) for **1**, 380 nm ($\lambda_{ex} = 305$ nm) for **2**, 360 nm ($\lambda_{ex} = 289$ nm) for **3**, as well as 386 nm ($\lambda_{ex} = 336$ nm) for **4**, respectively. These emission bands are greatly similar to the free Hmdpt emission for the π–π^* or n–π^* intra-ligand transition (Sun et al., 2013; Wenger, 2013; Zou et al., 2013; Chen et al., 2017). In contrast to the Hmdpt, the emissions of four CPs have the similar blue shifts, which are considered to be the energy transfer from the Hmdpt ligand to the Cd(II) centers for the ligand-to-metal charge transfer (LMCT) (Cao et al., 2017).

CONCLUSION

In summary, four new CPs with rigid Hmdpt and different benzendicarboxylate linkers have been successfully obtained. The different auxiliary carboxylates resulted in a series of new various structural CPs. Complex **1** has a 2-fold interlocked ***NbO*** net; **2** presents the 2D three-connected ***hcb*** net; **3** shows the double-insertion 3D ***fsh*** supramolecular network; and **4** displays a 3D eight-connected ***sqc117*** net. The CH_4/CO_2 sorption behaviors of **1** and **4** have been carefully carried out at different temperatures. Remarkably, complex **4** has preferable sorption and high CO_2 selectivity, making it as a useful gas storage/separation functional material.

DATA AVAILABILITY STATEMENT

The datasets presented in this study can be found in online repositories. The names of the repository/repositories and accession number(s) can be found in the article/**Supplementary Material**.

AUTHOR CONTRIBUTIONS

All authors listed have made a substantial, direct and intellectual contribution to the work, and approved it for publication.

FUNDING

This work was supported by the NSFC (21801111 and 22071194), Project of Central Plains Science and Technology Innovation Leading Talents of Henan Province (204200510001), and NSF of Shaanxi Province (2019JM-013).

SUPPLEMENTARY MATERIAL

The Supplementary Material for this article can be found online at: https://www.frontiersin.org/articles/10.3389/fchem.2020.616468/full#supplementary-material

REFERENCES

Bezuidenhout, C., Smith, V., Bhatt, P., Esterhuysen, C., and Barbour, L. (2015). Extreme carbon dioxide sorption hysteresis in open-channel rigid metal-organic frameworks. *Angew. Chem. Int. Ed.* 54, 2079–2083. doi: 10.1002/anie.201408933

Bhattacharya, B., Layek, A., Alam, M., Maity, D. K., Chakrabarti, S., Ray, P. P., et al. (2014). Cd(II) based metal-organic framework behaving as a Schottky barrier diode. *Chem. Commun.* 50, 7858–7861. doi: 10.1039/c4cc00827h

Bhattacharya, B., Maity, D. K., Layek, A., Jahiruddin, S., Halder, A., Dey, A., et al. (2016). Multifunctional mixed ligand metal organic frameworks: X-ray structure, adsorption, luminescence and electrical conductivity with theoretical correlation. *CrystEngComm.* 18, 5754–5763. doi: 10.1039/C6CE01173J

Biswas, S., Couck, S., Denysenko, D., Bhunia, A., Grzywa, M., Denayer, J., et al. (2013). Sorption and breathing properties of difluorinated MIL-47 and Al-MIL-53 frameworks. *Micropor. Mesopor. Mat.* 181, 175–181. doi: 10.1016/j.micromeso.2013.07.030

Blandez, J. F., Portillo, A. S., Navalón, S., Álvaro, M., Horcajada P, and García, H. (2016). Influence of functionalization of terephthalate linker on the catalytic activity of UiO-66 for epoxide ring opening. *J. Mol. Cat. A Chem.* 425, 332–339. doi: 10.1016/j.molcata.2016.10.022

Boldog, I., Domasevitch, K., Baburin, I., Ott, H., Gil-Hernandez, B., Sanchiz, J., et al. (2013). A rare alb-4,8-Cmce metal-coordination network based on tetrazolate and phosphonate functionalized 1,3,5,7-tetraphenyladamantane. *CrystEngComm.* 15, 1235–1243. doi: 10.1039/C2CE26819A

Cao, L., Li, H., Xu, H., Wei, Y., and Zang, S. (2017). Diverse dissolution-recrystallization structural transformations and sequential Förster resonance energy transfer behavior of a luminescent porous Cd-MOF. *Dalton Trans.* 46, 11656–11663. doi: 10.1039/C7DT02697H

Chen, D., Ma, X., Shi, W., and Cheng, P. (2015). Solvent-induced topological diversity of two Zn(II) metal-organic frameworks and high sensitivity in recyclable detection of nitrobenzene. *Cryst. Growth Des.* 15, 3999–4004. doi: 10.1021/acs.cgd.5b00614

Chen, S. S., Qiao, R., Sheng, L. Q., Zhao, Y., Yang, S., Chen, M. M., et al. (2013). Cadmium(II) and zinc(II) complexes with rigid 1-(1H-imidazol-4-yl)-3-(4H-tetrazol-5-yl)benzene and varied carboxylate ligands. *CrystEngComm.* 15, 5713–5725. doi: 10.1039/C3CE40150B

Chen, W., Lin, Y., Zhang, X., Xu, N., and Cheng, P. (2017). A new cadmium-organic framework fluorescent sensor for Al3+ and Ca2+ ions in aqueous medium. *Inorg. Chem. Commun*. 79, 29–32. doi: 10.1016/j.inoche.2017.03.010

Chou, C., Hu, F., Wu, K., Duan, T., Chi, Y., Liu, S., et al. (2014). 4,4′,5,5′-Tetracarboxy-2,2′-bipyridine Ru(II) sensitizers for dye-sensitized solar cells. *Inorg. Chem*. 53, 8593–8599. doi: 10.1021/ic501178f

DeFuria, M. D., Zeller, M., and Genna, D. T. (2016). Removal of pharmaceuticals from water via π-π stacking interactions in perfluorinated metal–organic frameworks. *Cryst. Growth Des*. 16, 3530–3534. doi: 10.1021/acs.cgd.6b00488

Dey, A., Bairagi, D., and Biradha, K. (2017). MOFs with PCU topology for the inclusion of one-dimensional water cages: selective sorption of water vapor, CO_2, and dyes and luminescence properties. *Cryst. Growth Des*. 17, 3885–3892. doi: 10.1021/acs.cgd.7b00502

Du, L., Wang, H., Liu, G., Xie, D., Guo, F., Hou, L., et al. (2015). Structural diversity of five new bitriazole-based complexes: luminescence, sorption, and magnetic properties. *Dalton Trans*. 44, 1110–1119. doi: 10.1039/C4DT03129F

Esfandiari, K., Ghoreyshi, A., and Jahanshahi, M. (2017). Using artificial neural network and ideal adsorbed solution theory for predicting the CO_2/ch4 selectivities of metal-organic frameworks: a comparative study. *Ind. Eng. Chem. Res*. 56, 14610–14622. doi: 10.1021/acs.iecr.7b03008

Han, G., Wang, K., Peng, Y., Zhang, Y., Huang, H., and Zhong, C. (2017). Enhancing higher hydrocarbons capture for natural gas upgrading by tuning van der waals interactions in fcu-type Zr-MOFs. *Ind. Eng. Chem. Res*. 56, 14633–14641. doi: 10.1021/acs.iecr.7b03341

Handke, M., Weber, H., Lange, M., Mollmer, J., Lincke, J., Glaser, R., et al. (2014). Network flexibility: control of gate opening in an isostructural series of Ag-MOFs by linker substitution. *Inorg. Chem*. 53, 7599–7607. doi: 10.1021/ic500908r

Hiraide, S., Tanaka, H., Ishikawa, N., and Miyahara, M. (2017). Intrinsic thermal management capabilities of flexible metal-organic frameworks for carbon dioxide separation and capture. *ACS Appl. Mater. Interfaces* 9, 41066–41077. doi: 10.1021/acsami.7b13771

Hong, X. J., Wei, Q., Cai, Y. P., Zheng, S. R., Yu, Y., Fan, Y. Z., et al. (2017). 2-fold interpenetrating bifunctional Cd-metal-organic frameworks:highly selective adsorption for CO2 and sensitive luminescent sensing of nitro aromatic 2,4,6-trinitrophenol. *ACS Appl. Mater. Interfaces* 9, 4701–4708. doi: 10.1021/acsami.6b14051

Hu, F., Shi, Y., Chen, H., and Lang, J. (2015). A Zn(II) coordination polymer and its photocycloaddition product: syntheses, structures, selective luminescence sensing of iron(III) ions and selective absorption of dyes. *Dalton Trans*. 44, 18795–18803. doi: 10.1039/C5DT03094C

Ichikawa, M., Kondo A; Noguchi, H., Kojima, N., Ohba, T., H., Kajiro H, Hattori, Y., et al. (2016). Double-step gate phenomenon in CO_2 sorption of an elastic layer-structured MOF. *Langmuir* 32, 9722–9726. doi: 10.1021/acs.langmuir.6b02551

Islamoglu, T., Goswami, S., Li, Z. Y., Howarth, A. J., Farha, O. K., and Hupp, J. T. (2017). Postsynthetic tuning of metal-organic frameworks for targeted applications. *Acc. Chem. Res*. 50, 805–813. doi: 10.1021/acs.accounts.6b00577

Jin, J., Wu, J., Yang, G., Wu, Y., and Wang, Y. (2016). A microporous anionic metal-organic framework for a highly selective and sensitive electrochemical sensor of Cu2+ ions. *Chem. Commun*. 52, 8475–8478. doi: 10.1039/C6CC03063G

Ju, P., Jiang, L., and Lu, T. (2015). A three-dimensional dynamic metal-organic framework with fourfold interpenetrating diamondoid networks and selective adsorption properties. *Inorg. Chem*. 54, 6291–6295. doi: 10.1021/acs.inorgchem.5b00592

Ju, Z. F., Yan, S. C., and Yuan, D. Q. (2016). *De novo* tailoring pore morphologies and sizes for different substrates in a urea-containing MOFs catalytic platform. *Chem. Mater*. 28, 2000–2010. doi: 10.1021/acs.chemmater.5b03999

Kariem, M., Kumar, M., Yawer, M., and Sheikh, H. N. (2017). Solvothermal synthesis and structure of coordination polymers of Nd(III) and Dy(III) with rigid isophthalic acid derivatives and flexible adipic acid. *J. Mol. Struct*. 1150, 438–446. doi: 10.1016/j.molstruc.2017.08.111

Kumar, P., Paul, A., and Deep, A. (2014). A luminescent nanocrystal metal organic framework for chemosensing of nitro group containing organophosphate pesticides. *Anal. Methods*. 6, 4095–4101. doi: 10.1039/C3AY42189A

Lannoeye, J., Voorde, B. V., Bozbiyik, B., Reinsch, H., Denayer, J., and Vos, D. D. (2016). An aliphatic copper metal-organic framework as versatile shape selective adsorbent in liquid phase separations. *Microp. Mesop. Mater*. 226, 292–298. doi: 10.1016/j.micromeso.2016.01.044

Li, J., Yang, G., Wei, S., Gao, R., Bai, N., and Wang, Y. (2015). Two microporous metal-organic frameworks with suitable pore size displaying the high CO2/CH4 selectivity. *Cryst. Growth Des*. 15, 5382–5387. doi: 10.1021/acs.cgd.5b00997

Li, J. X., Li, Y. F., Liu, L. W., and Cui, G. H. (2018). Luminescence, electrochemical and photocatalytic properties of sub-micron nickel(II) and cobalt(II) coordination polymers synthesized by sonochemical process. *Ultrason. Sonochem*. 41, 196–205. doi: 10.1016/j.ultsonch.2017.09.039

Li, N., Chang, Z., Huang, H., Feng, R., He, W. W., Zhong, M., et al. (2019). Specific K+ binding sites as CO2 traps in a porous MOF for enhanced CO_2 selective sorption. *Small* 15:1900426. doi: 10.1002/smll.201900426

Li, P. Z., Wang, X. J., Liu, J., Lim, J. S., Zou, R. Q., and Zhao, Y. L. (2016). A triazole-containing metal-organic framework as a highly effective and substrate size-dependent catalyst for CO_2 conversion. *J. Am. Chem. Soc*. 138, 2142–2145. doi: 10.1021/jacs.5b13335

Li, X. Y., Shi, W. J., Wang, X. Q., Ma, L. N., Hou, L., and Wang, Y. Y. (2017). Luminescence modulation, white light emission, and energy transfer in a family of lanthanide metal-organic frameworks based on a planar π-conjugated ligand. *Cryst. Growth Des*. 17, 4217–4224. doi: 10.1021/acs.cgd.7b00530]

Liang, L., Yang, C., Ma, Y., and Deng, H. (2013). In situ hydrothermal syntheses of five new cadmium(II) coordination polymers based on 3-(1H-tetrazol-5-yl)benzoate ligand. *CrystEngComm*. 15, 365–375. doi: 10.1039/C2CE26720A

Lim, K., Jeong, S., Kang, D., Song, J., Jo, H., Lee, W., et al. (2017). Luminescent metal-organic framework sensor: exceptional Cd2+ turn-on detection and first *in situ* visualization of Cd2+ ion diffusion into a crystal. *Chem. Eur. J*. 23, 4803–4809. doi: 10.1002/chem.201604252

Lin, J. B., Lin, R. B., Cheng, X. N., Zhang, J. P., and Chen, X. M. (2011). Solvent/additive-free synthesis of porous/zeolitic metal azolate frameworks from metal oxide/hydroxidew. *Chem. Commun*. 47, 9185–9187. doi: 10.1039/C1CC12763B

Lin, J. B., Zhang, J. P., and Chen, X. M. (2010). Nonclassical active site for enhanced gas sorption in porous coordination polymer. *J. Am. Chem. Soc*. 132, 6654–6656. doi: 10.1021/ja1009635

Lin, Y., Zhang, X., Chen, W., Shi, W., and Cheng, P. (2017). Three cadmium coordination polymers with carboxylate and pyridine mixed ligands: luminescent sensors for Fe(III) and Cr(VI) ions in an aqueous medium. *Inorg. Chem*. 56, 11768–11778. doi: 10.1021/acs.inorgchem.7b01790

Liu, B., Li, Y., Hou, L., Yang, G., Wang, Y., and Shi, Q. (2013). Dynamic Zn-based metal-organic framework: stepwise adsorption, hysteretic desorption and selective carbon dioxide uptake. *J. Mater. Chem. A*. 1, 6535–6538. doi: 10.1039/C3TA10918F

Liu, J. Y., Wang, Q., Zhang, L. J., Y. B., Xu, Y. Y., Zhang X, Zhao, C. Y., et al. (2014). Anion-exchange and anthracene-encapsulation within copper(II) and manganese(II)-triazole metal-organic confined space in a single crystal-to-single crystal transformation fashion. *Inorg. Chem*. 53, 5972–5985. doi: 10.1021/ic500183b

Lu, N. Y., Zhou, F., Jia, H. H., Wang, H. Y., Fan, B. B., and Li, R. F. (2017). Dry-gel conversion synthesis of Zr-based metal-organic frameworks. *Ind. Eng. Chem. Res*. 56, 14155–14163. doi: 10.1021/acs.iecr.7b04010

Manna, B., Desai, A. V., and Ghosh, S. K. (2016). Neutral N-donor ligand based flexible metal-organic frameworks. *Dalton Trans*. 45, 4060–4072. doi: 10.1039/C5DT03443D

Pachfule, P., and Banerjee, R. (2011). Porous nitrogen rich cadmium-tetrazolate based Metal Organic Framework (MOF) for H2 and CO2 uptake. *Cryst. Growth Des*. 11, 5176–5181. doi: 10.1021/cg201054f

Park, S. S., Hendon, C. H., Fielding, A. J., Walsh, A., Keeffe, M., and Dinca, M. (2017). The organic secondary building unit: strong intermolecular π interactions define topology in MIT-25, a mesoporous MOF with proton-replete channels. *J. Am. Chem. Soc*. 139, 3619–3622. doi: 10.1021/jacs.6b13176

Qin, L., Ju, Z., Wang, Z., Meng, F., Zheng, H., and Chen, J. (2014). Interpenetrated metal-organic framework with selective gas adsorption and luminescent properties. *Cryst. Growth Des*. 14, 2742–2746. doi: 10.1021/cg500269h

Rosa, I. M. L., Costa, M. C. S., Vitto, B. S., Amorim, L., Correa, C. C., Pinheiro, C. B., et al. (2016). Influence of synthetic methods in the structure and dimensionality of coordination polymers. *Cryst. Growth Des*. 16, 1606–1616. doi: 10.1021/acs.cgd.5b01716

Sheldrick, G. M. (1997). *SHELXL-97. Program for Refinement of Crystal Structures*. Gottingen: University of Göttingen.

Smith, M. K., Angle, S. R., and Northrop, B. H. (2015). Preparation and analysis of cyclodextrin-based metal-organic frameworks: laboratory experiments adaptable for high school through advanced undergraduate students. *J. Chem. Educ.* 92, 368–372. doi: 10.1021/ed500540t

Song, J. Y., Ahmed, I., Seo, P. W., and Jhung, S. H. (2016). UiO-66-type metal-organic framework with free carboxylic acid:versatile adsorbents via h-bond for both aqueous and nonaqueous phases. *ACS. Appl. Mater. Interfaces* 8, 27394–27402. doi: 10.1021/acsami.6b10098

Song, Y., Feng, M. L., Wu, Z. F., and Huang, X. Y. (2015). Solvent-assisted construction of diverse Mg-TDC coordination polymers. *CrystEngComm*. 17, 1348–1357. doi: 10.1039/C4CE02288B

Sun, D., Han, L., Yuan, S., Deng, Y., Xu, M., and Sun, D. (2013). Four new Cd(II) coordination polymers with mixed multidentate N-donors and biphenyl-based polycarboxylate ligands: syntheses, structures, and photoluminescent properties. *Cryst. Growth Des*. 13, 377–385. doi: 10.1021/cg301573c

Sun, Y., Hu, Z., Zhao, D., and Zeng, K. (2017). Probing nanoscale functionalities of metal-organic framework nanocrystals. *Nanoscale* 9, 12163–12169. doi: 10.1039/C7NR04245K

Waller, P. J., Gandara, F., and Yaghi, O. M. (2015). Chemistry of covalent organic frameworks. *Acc. Chem. Res*. 48, 3053–3063. doi: 10.1021/acs.accounts.5b00369

Wang, D., Liu, B., Yao, S., Wang, T., Li, G., Huo, Q., et al. (2015). A polyhedral metal-organic framework based on the supermolecular building block strategy exhibiting high performance for carbon dioxide capture and separation of light hydrocarbons. *Chem. Commun*. 51, 15287–15289. doi: 10.1039/C5CC06162H

Wang, H., Yi, F. Y., Dang, S., Tian, W. G., and Sun, Z. M. (2014). Rational assembly of Co/Cd-MOFs featuring topological variation. *Cryst. Growth Des*. 14, 147–156. doi: 10.1021/cg4013334

Wang, S., and Wang, X. C. (2015). Multifunctional metal-organic frameworks for photocatalysis. *Small* 11, 3097–3112. doi: 10.1002/smll.201500084

Wang, Z., Qin, L., Chen, J., and Zheng, H. (2016). H-bonding interactions induced two isostructural Cd(II) metal-organic frameworks showing different selective detection of nitroaromatic explosives. *Inorg. Chem*. 55, 10999–11005. doi: 10.1021/acs.inorgchem.6b01521

Wenger, O. (2013). Vapochromism in organometallic and coordination complexes: chemical sensors for volatile organic compounds. *Chem. Rev*. 113, 3686–3733 doi: 10.1021/cr300396p

Wheeler, S. E. (2013). Understanding substituent effects in noncovalent interactions involving aromatic rings. *Chem. Res*. 46, 1029–1038. doi: 10.1021/ar300109n

Wu, Y., Qian, J., Yang, G., Yang, F., Liang, Y., Zhang, W., et al. (2017). High CO2 uptake capacity and selectivity in a fascinating nanotube-based metal-organic framework. *Inorg. Chem*. 56, 908–913. doi: 10.1021/acs.inorgchem.6b02491

Xing, S., and Janiak, C. (2020). Design and properties of multiple-emitter luminescent metal–organic frameworks. *Chem. Commun*. 56, 12290–12306. doi: 10.1039/D0CC04733C

Yadav, V. N., and Gorbitz, C. H. (2013). A supramolecular 2:1 guanidinium-carboxylate based building block for generation of water channels and clusters in organic materials. *CrystEngComm*. 15, 439–442. doi: 10.1039/C2CE26572A

Yan, Y. T., Zhang, S. S., Yang, G. P., Zhang, W. Y., Zhang, F., Cao, F., et al. (2017). The influence of coordination modes and active sites of a 5-(triazol-1-yl) nicotinic ligand on the assembly of diverse MOFs. *Dalton Trans*. 46, 9784–9793. doi: 10.1039/C7DT01523B

Yao, R. X., Cui, X., Jia, X. X., Zhang, F. Q., and Zhang, X. M. (2016). A luminescent zinc(II) Metal-Organic Framework (MOF) with conjugated π-electron ligand for high iodine capture and nitroexplosive detection. *Inorg. Chem*. 55, 9270–9275. doi: 10.1021/acs.inorgchem.6b01312

Ye, R., Zhang, X., Zhai, J., Qin, Y., Zhang, L., Yao, Y., et al. (2015). N-donor ligands enhancing luminescence properties of seven Zn/Cd(II) MOFs based on a large rigid π-conjugated carboxylate ligand. *CrystEngComm*. 17, 9155–9166. doi: 10.1039/C5CE01884F

Zhang, S., Jiang, F., Wu, M., Chen, L., Luo, J., and Hong, M. (2013). pH modulated assembly in the mixed-ligand system Cd(II)-dpstc-phen: structural diversity and luminescent properties. *CrystEngComm*. 15, 3992–4002. doi: 10.1039/C3CE27108K

Zhang, X., Chen, Z., Liu, X., Hanna, S. L., Wang, X., Taheri-Ledari, R., et al. (2020). A historical overview of the activation and porosity of metal–organic frameworks. *Chem. Soc. Rev*. 49, 7406–7427. doi: 10.1039/D0CS00997K

Zhang, X., Zhou, J., Shi, W., Zhang, Z., and Cheng, P. (2013). Two cadmium(II) coordination polymers constructed by carboxylate and pyridine mixed ligands: synthesis, structure and luminescent properties. *CrystEngComm*. 15, 9738–9744. doi: 10.1039/C3CE41073K

Zou, J. Y., Gao, H. L., Shi, W., Cui, J. Z., and Cheng, P. (2013). Auxiliary ligand-assisted structural diversities of three metal-organic frameworks with potassium 1H-1,2,3-triazole-4,5 -dicarboxylic acid: syntheses, crystal structures and luminescence properties. *CrystEngComm*. 15, 2682–2687. doi: 10.1039/C3CE26854C

Conflict of Interest: The authors declare that the research was conducted in the absence of any commercial or financial relationships that could be construed as a potential conflict of interest.